Polymer 50 (2009) 3259–3268

Contents lists available at ScienceDirect

Polymer

journal homepage: www.elsevier.com/locate/polymer

Methacrylate/acrylate ABA triblock copolymers by atom transfer radical polymerization; their properties and application as a mediator for organically dispersible gold nanoparticles

Haimanti Datta, Anil K. Bhowmick, Nikhil K. Singha*

Rubber Technology Centre, Indian Institute of Technology, Kharagpur 721302, India

ARTICLE INFO

Article history:
Received 16 October 2008
Received in revised form
1 April 2009
Accepted 22 April 2009
Available online 9 May 2009

Keywords:
Atom transfer radical polymerization
Block copolymers
Gold nanoparticle

ABSTRACT

This investigation reports the preparation of a series of well-defined Poly(methyl methacrylate)-*b*-poly-(hexyl acrylate)-*b*-poly (methyl methacrylate) (PMMA-*b*-PHA-*b*-PMMA) triblock copolymers by Atom Transfer Radical Polymerization (ATRP). Their morphology, dynamic mechanical and tensile properties are thoroughly investigated. Phase separation is observed for all the above-mentioned triblock copolymers, which contain PMMA outer blocks in the molecular weight (M_n) range of 10,000–80,000 and PHA inner blocks with M_n in the range 20,000–40,000. The dynamic mechanical measurements essentially reveal two glass transitions and an intermediate flat rubbery plateau in between. Tensile studies indicate that as the PMMA content increases, there is an increase in tensile strength and decrease in elongation at break, which is the case for most of the thermoplastic elastomers (TPE). Eventually, the as prepared block copolymers (with PMMA content 50–80%) offer to be an effective stabilizer for preparing gold nanoparticle aggregates, the shape and size of which can be modulated by tuning the block copolymer composition. The formation of nanoparticle aggregates and their possible non-covalent interaction with the base polymer has been substantiated by UV–vis analysis, transmission electron microscopy, energy-dispersive X-ray spectroscopy, dynamic light scattering and Fourier transform infrared spectroscopy.

1. Introduction

Block copolymers constituting polymer blocks of different properties, such as solubility and glass transition temperature (T_g) have received much consideration from the viewpoint of materials applications including compatibilizers in polymer blends, adhesives and thermoplastic elastomers (TPEs) [1,2]. The increasing importance of block copolymers arises mainly from their unique properties in solution and in the solid state, which is a consequence of their molecular structure [3]. The acrylate–methacrylate block copolymers are not only challenging to be prepared synthetically but are also interesting owing to their well-tuned morphological, phase and mechanical properties [4,5]. This is because of the drawback of the conventional diene based TPEs as displayed by their poor oxidation resistance of the unsaturated central block and relatively low service temperature (60–70 °C) in relation to the glass transition temperature (T_g) of polystyrene [4b]. In acrylate based systems, depending on the alkyl substituent of the ester group, one can manipulate the T_g to tune it over a wide temperature range (−65 to 200 °C). The much better resistance of polyacrylates to UV and oxidation compared to polydienes is an additional advantage, opening new applications e.g., in the automotive market. With the recent advances in the field of controlled radical polymerizations, atom transfer radical polymerization (ATRP) has emerged as an attractive tool to prepare these all acrylate based block copolymers rather easily and their properties can be tuned without extra precautions [6]. It has been well documented that except in the case of small alkyl groups and low molecular weights, poly (alkyl methacrylates) and poly (alkyl acrylates) are immiscible [5d]. Preparation of well-defined (meth)acrylic block starting from the polyacrylate dormant species is quite challenging because of the slower activation of dormant polyacrylate chain end to a radical species compared to the activation of a dormant methacrylate chain end [7]. The result is the slow initiation of the macroinitiator, which leads to poor control of molecular weight (i.e., broad polydispersity and/or bimodality). Matyjaszewski et al. [5c], however, reported the one-pot synthesis of mixed acrylate block copolymers (polybutylacrylate–polymethylmethacrylate) using halogen exchange technique so that the rate of cross propagation should be comparable to the rate of the subsequent propagation reaction. The

* Corresponding author. Tel.: +91 3222 283178; fax: +91 3222 282700.
E-mail address: nks@rtc.iitkgp.ernet.in (N.K. Singha).

0032-3861/$ – see front matter © 2009 Elsevier Ltd. All rights reserved.
doi:10.1016/j.polymer.2009.04.071

literature survey reveals that the in depth investigation of acrylate–methacrylate block copolymers (by ATRP) have not been reported yet for the acrylates having alkyl chain length >C4.

With reference to our earlier interest in the ATRP of different acrylates having different alkyl chain length as well as different functional groups [8], herein, we report the preparation of a series of triblock copolymers of various molecular weights and compositions by ATRP using poly (hexyl acrylate) (PHA) ($C = 6$) ($T_g = -57\,^{\circ}C$) as the soft middle block and poly (methyl methacrylate) (PMMA) ($T_g = 100\,^{\circ}C$) as the hard outer blocks (i.e., PMMA-*b*-PHA-*b*-PMMA, further abbreviated as MHM). The synthetic strategy was based on starting from difunctional PHA macroinitiator, acrylate–methacrylate triblocks were prepared by halogen exchange technique. An in depth structure–property correlation have been investigated by size exclusion chromatography (SEC), differential scanning calorimetry (DSC), dynamic mechanical thermal analysis (DMTA), tensile properties and atomic force microscopy (AFM).

Block copolymers have been used to stabilize a variety of nanoparticle materials by forming steric or ionic barriers around the particles [9–16]. Gold nanoparticles (AuNPs) exhibit numerous applications ranging from optoelectronics to catalysis that differ significantly from those of their corresponding bulk materials [17–20]. Again, assembly of individual nanoparticles into ensembles has recently become a widely pursued objective [21,22]. Henceforth, it is interesting to produce and study the interparticle interactions while the particles are held together by weak forces in an aggregate [23]. The ability for very sensitive and spatially confined molecular structural probing makes gold nanoparticle aggregates as very promising tools for studies of small structures in biological materials, such as cellular compartments [22].

As revealed by literature survey, the polymers used as stabilizer in synthesizing AuNPs were mostly amphiphilic; the synthesis method was primarily based on templating of AuNPs inside the spherical micelle core. Examples include poly(ethyleneoxide)-*b*-poly(propyleneoxide)-*b*-poly(ethyleneoxide) [24], polyethylene glycol-*b*-polycaprolactone [25], poly (ethyleneoxide)-*b*-polycaprolactone) [26], poly(styrene)-*b*-poly(2-vinylpyridine) [27], poly (methylmethacrylate)-*b*-poly[2-(N,N-dimethylamino) ethyl methacrylate] [28] etc.

However, till date, there has been no report on the use of non-amphiphilic block copolymers to synthesize and confine metal nanoparticles in aggregates. In this present study, we explored the role of "all-acrylate" hydrophobic block copolymers as a mediator for synthesis of gold nanoparticle aggregates for the first time. Nanoscale aggregation of gold in an organic solvent is an important addition to the hitherto predominantly water based processes for assembling nanoparticles inside the polymer surfactant.

2. Experimental section

2.1. Materials

The monomers, hexyl acrylate (HA) (Aldrich, 98 %), methyl methacrylate (MMA) (Aldrich, 97%) were passed through an alumina column, distilled under reduced pressure over calcium hydride and then were stored at $-4\,^{\circ}C$ under nitrogen. Acetone, tetrahydrofuran and *p*-xylene were distilled over molecular sieves under vacuum. CuBr and CuCl were stirred with glacial acetic acid for 12 h, washed with ethanol and diethyl ether, and then was dried under vacuum at 75 °C for 3 days. N, N, N′, N″, N″-pentamethyldiethylenetriamine (PMDETA) (Aldrich, 99%), 1, 1, 4, 7, 10, 10-hexamethyltriethylenetetramine (HMTETA) (Aldrich, 97%) and all other chemicals were used as received. The difunctional initiator 1,2-bis(bromopropinyloxy)ethane (BBPE) was prepared according to the literature method [29]. Details of the preparative method of the difunctional initiator, α,ω-Dibromo-PHA (Br-PHA-Br) has been described elsewhere [8c].

All the other reagents like tetrachloroauric acid ($HAuCl_4$) (Fluka, purum), sodium boro hydride ($NaBH_4$) (Merck), dimethyl formamide (Fluka, pure grade) etc. were used as received.

2.1.1. Preparation of ABA triblock copolymer

A typical example is given here for preparing a triblock copolymer of composition 20-20-20. The difunctional PHA macroinitiator (0.995 g, 4.97×10^{-5} mol) ($M_n = 20{,}000$, $M_w/M_n = 1.23$) and CuCl (0.0049 g, 4.97×10^{-5} mol) were added into a test tube provided with a rubber septum and then MMA (2 g, 1.99×10^{-2} mol) was injected into the vessel followed by the addition of HMTETA (0.0114 g, 4.97×10^{-5} mol), under nitrogen atmosphere. The mixture was stirred at room temperature for 5 min and the vessel was then placed in an oil bath at 90 °C with constant stirring. A conversion of 95% was reached at 2 h. The polymer was purified by passing through alumina column, then precipitated into a mixture of methanol/water and finally isolated by vacuum filtration. After drying under vacuum for 12 h, ^1H NMR analysis was performed in $CDCl_3$.

For mechanical and rheological measurements, films were cast from a solution of the MHM copolymer (12.5% w/v, 6 mL) in THF onto a clean polyethylene petri dish (100 mm diameter). The solvent was let to evaporate for 24 h at room temperature. The films were dried at 160 °C for 3 days in a vacuum oven in order to remove the last traces of solvent and then quenched to room temperature.

2.1.2. Preparation of Au nanoparticles stabilized by MHM triblock copolymer

Au nanoparticles were prepared by reducing $HAuCl_4$ with $NaBH_4$ using MHM triblock copolymer as stabilizing matrix. The block copolymers were dissolved in DMF at a concentration of 1 g/L. A known amount of a $HAuCl_4$ solution in DMF ($c = 10$ g/L) was then added to the copolymer solution, and the mixture was stirred for 1 h at 30 °C. Since $HAuCl_4$ molecules are expected to be essentially located at the neighboring site of PMMA segment of the MHM triblock copolymer, the critical parameter to control is the $HAuCl_4$/PMMA molar ratio. In preliminary experiments, we have varied this ratio from 1:1 to 1:2, 1:4, and 1:10. A known amount of a $NaBH_4$ solution in DMF was then added to the copolymer loaded with $HAuCl_4$ in each composition. The $HAuCl_4/NaBH_4$ molar ratio was also varied. The best results were obtained with a $HAuCl_4$/PMMA molar ratio of 1:4 and $HAuCl_4/NaBH_4$ molar ratio of 1:2. The color of the gold precursor-loaded polymers then immediately turned from yellow into bluish purple or deep blue, indicating the occurrence of nanoaggregation.

2.1.3. Preparation of the MHM–Au nanocomposite

Previously prepared MHM–Au colloids (5 mL) in DMF was directly added to a solution of PMMA-*b*-PHA-*b*-PMMA (0.25 g; $M_n = 60{,}000$), dissolved in the same solvent (5 mL), and stirred gently for 10 h. The MHM–Au/MHM solution was concentrated by the slow evaporation of DMF at 80 °C for 48 h. The resulting concentrated solution was casted onto a glass slide and dried at room temperature for 2 days and then vacuum-dried to obtain a transparent film.

2.2. Characterization

2.2.1. Gel permeation chromatography (GPC)

Molecular weights and molecular weight distributions of the polymers were determined by size exclusion chromatography (SEC) at ambient temperature using a Viscotek Gel Permeation

Chromatography equipped with a VE 1122 solvent delivery system, a VE 3580 RI detector, and two VIscoGEL mixed bed columns (17392-GMHHRM), which were preceded by a guard column. Data analysis was collected using OmniSEC 4.2 software. THF was used as the eluent at a flow rate of 1.0 ml/min and calibration was carried out using low polydispersity poly (methyl methacrylate) standards. Before injection into the GPC system, the polymer solutions were treated with cation exchange resin Dowex 50 W (Fluka) to free from Cu salts.

2.2.2. Nuclear magnetic resonance spectrometry (NMR)

^{1}H NMR spectra were recorded on a Bruker AM 300 MHz spectrometer at room temperature using $CDCl_3$ as solvent and TMS as internal reference.

2.2.3. Differential scanning calorimetry (DSC)

Differential scanning calorimetry measurements were performed in a TA DSC instrument (model Q100V 8.1), working under nitrogen atmosphere. The temperature scale as well as the latent heat was calibrated with indium. Samples ($\sim$10 mg) were first made homogeneous by heating and cooling once to erase out the preparation history and finally scanned from -100 to $+180$ °C at a heating rate of 10 °C/min. The glass transition temperature (T_g) was taken from the second scan to ensure reproducible thermograms.

2.2.4. Dynamic mechanical thermal analysis (DMTA)

Dynamic mechanical properties were measured using a dynamic mechanical analyzer (DMA Q800, TA Instruments). The temperature sweep experiments were carried out at the frequency of 1 Hz (at strain 1% and at a heating rate 2 °C/min) holding the film with a film tension clamp. Loss tangent ($\tan\delta$) was measured as a function of temperature for all the samples under identical conditions.

2.2.5. Tensile tests

Tensile properties were measured using a universal testing machine (Z010, Zwick Roell, Ulm, Germany) at a crosshead speed of 100 mm/min at 25 °C. Tensile specimens were punched from cast sheets with ASTM Die-C. The average of three tests is reported here. TestXpert II software (Zwick Roell Ulm, Germany) was used for data acquisition and analysis.

2.2.6. Fourier transform infrared spectroscopy (FTIR)

FTIR spectra were recorded using a Perkin Elmer FTIR-spectrophotometer (model spectrum RX-I), within a range of 400–4400 cm^{-1} using a resolution of 4 cm^{-1}. An average of 16 scans has been recorded for each sample.

2.2.7. Atomic force microscopy (AFM)

2.2.7.1. Sample preparation. Thin MHM films ($\sim$600 nm thick) of the samples were cast on freshly cleaved mica foil from a dilute solution of the polymer in THF (12 mg/mL) by slow evaporation of THF. This was done inside a dessicator saturated with THF vapor and provided with an outlet fitted with a stopcock. The films were then dried at 160 °C in a vacuum oven for 72 h after which the vacuum was released by letting in air through a sintered glass filter and the films were immediately taken out of the oven. Before doing AFM, one representative sample (with 66% PMMA content) was annealed at 140 °C for 24 h in vacuum.

2.2.7.2. Measurements. The AFM measurements were performed in the "soft tapping mode" (TMAFM) using a Nanoscope IIIa microscope (Veeco, Inc) operated at room temperature in air. Images were recorded from different area of each sample, and the time for scanning was ca. 5 min. The images were digitally sampled at the maximum number of pixels (512) in each direction, and the Nanoscope image processing software was used for image analysis. Unless otherwise stated, image treatment was limited to a "flattening" operation, whereby a first-order surface representing height variations related to a possible tilt of the sample, is subtracted from the original image.

2.2.8. UV–Vis spectroscopy

The visible absorption spectra of the Au nanoparticles as prepared in solution and the polymer–Au nanocomposite films were recorded with the aid of a Hewlett–Packard diode-array UV–vis spectrophotometer (HP 8453) at room temperature.

2.2.9. Transmission electron microscopy (TEM)

Transmission electron microscopy (TEM) images were obtained on a JEOL 2000 electron microscope equipped with a Gatan video camera and a Gatan Multiscan CCD camera (1024 $\times$ 1024 pixels). TEM samples were prepared by dropping nanoparticle solutions (5 μL) onto carbon coated copper grids (300 mesh, Electron Microscopy Science) followed by air drying. All TEM images were obtained at an operating voltage of 200 kV.

2.2.10. Thermogravimetric analysis (TGA)

Thermogravimetric analysis of neat polymer and the hybrid composites were recorded with a DuPont TGA instrument (Model no. 2000). The measurements were performed from ambient temperature to 600 °C at a programmed heating rate of 20 °C/min under nitrogen atmosphere. A sample weight of ca.10 mg was taken for all the measurements.

2.2.11. Dynamic light scattering (DLS)

Dynamic light scattering measurement of the suspension of polymer-stabilized AuNPs was performed by using a Zetasizer Nano ZS (Malvern Instruments) containing a He–Ne laser operating at an incident wavelength of 652 nm.

3. Results and discussion

3.1. Preparation of ABA block copolymers

ATRP can be applied to block copolymer synthesis in two ways. The first is the simple addition of a second monomer to the reaction medium after nearly complete consumption of the first monomer. The second method involves the isolation and purification of the first polymer, then using it as a macroinitiator. Although the first method is easy to operate, there is a chance of formation of statistical, instead of pure block copolymers. Herein, we prepared "all-acrylate" triblock copolymers according to the second approach. In the first step, α,ω-dibromo-PHA was synthesized which then was used as the macroinitiator in the second stage for the synthesis of MHM triblock copolymers following the halide exchange technique. The difunctional macroinitiator of M_n 20,000 with PDI of 1.23, thus obtained, was used to prepare a series of the MHM triblock copolymers with varying end blocks (sample a–d, Table 1). Effect of the variation of middle block length has also been investigated (sample e, Table 1). Table 1 summarizes the main molecular characteristics of the triblocks those have been prepared accordingly.

Fig. S1 (in Supplementary section) shows a ^{1}H NMR spectrum of a representative MHM triblock copolymer (sample a, Table 1). The compositional analysis of the blocks is made on the basis of the calculation of the relative intensity of resonances for the –OCH_3 protons of PMMA (at 3.6 ppm) and –OCH_2–protons of the PHA (at 4.0 ppm). The number average molecular weight (M_n) of the parent

Table 1
Molecular characterization details of the triblock copolymers.

Sample	Br-PHA-Br		PMMA-*b*-PHA-*b*-PMMA			
	M_n^{SEC}	M_w/M_n	M_n^{SEC}	M_w/M_n	% PMMA (wt.%)	M_n^{NMR} ($\times 10^{-3}$)
a	20 K	1.23	30 K	1.21	33	5-20-5
b	20 K	1.23	40 K	1.20	50	10-20-10
c	20 K	1.23	60 K	1.18	66	20-20-20
d	20 K	1.23	100 K	1.18	80	40-20-40
e	40 K	1.25	80 K	1.20	50	20-40-20

MHM triblocks is calculated from the copolymer composition and molecular weight of the first difunctional PHA. The composition so determined agrees well with that calculated from the amount of PHA used and MMA consumed during the synthesis of the copolymers.

3.2. Dynamic mechanical properties

To investigate the phase behavior of block copolymers, DMTA measurements have been performed. Figs. 1 and 2 illustrate the thermal dependence of the dynamic storage modulus (E′) and loss factor (tan δ) respectively in the temperature range from −100 to 200 °C for a series of MHM triblock copolymers of varying compositions. Summary of the dynamic mechanical properties of the triblocks has been displayed in Table 2. Two glass transitions and an intermediate rubbery plateau are observed for all copolymers, which are in agreement with extended phase separation, where PMMA blocks form the glassy domains, connecting the flexible PHA blocks [4a,4b,30–32]. The transition at low temperature (T_gI) is assigned to the glass transition temperature of the soft PHA block, whereas the high temperature transition (T_gII) corresponds to the PMMA rich phase [33].

Intermediate between two transitions, the very flat plateau indicates that the physical network of PHA chains is essentially free from undesirable diblocks (PMMA–PHA) or homopolymers. The height of the plateau depends strongly on the PMMA content: E′ ∼ 7 Pa when PMMA is 33% (sample a) and E′ ∼ 8.7 Pa, when PMMA is 80% (sample d) by weight. For the sample with very short PMMA chain (sample a) the plateau is reasonably short. At ∼80 °C, E′ drops rapidly, which corresponds to the terminal zone as is commonly observed in traditional hard–soft–hard diene based triblock copolymers and attributed to the failure of the shorter chains to get involved in the formation of three dimensional networks of rubbery chains [30]. The increase of M_n of PMMA from 10 K to 20 K changes the situation as designated by curve b. Here,

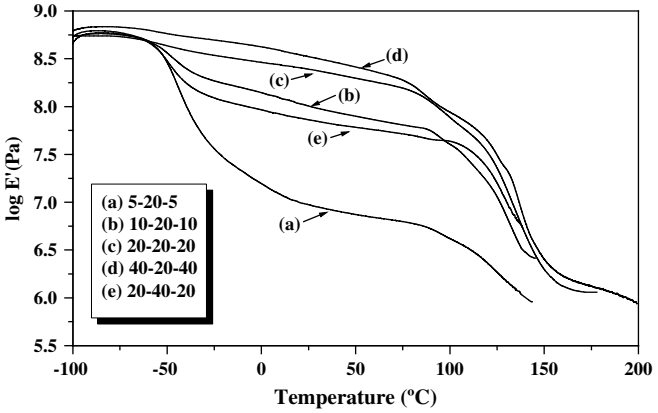

Fig. 1. Storage modulus (E′) as a function of temperature for MHM.

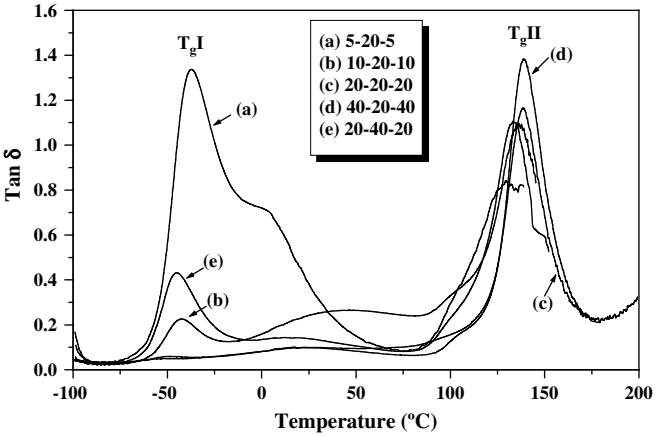

Fig. 2. tan δ as a function of temperature for MHM samples.

onset of the terminal zone is registered at ∼89 °C, thus 9 °C higher than for sample a. A substantial improvement of the upper service temperature is observed in the case of 20-40-20 (sample e), where the particular onset temperature arises at ∼102 °C, attributed to the longer middle block length. Except in the case of high PMMA content (sample c and d), the E′ measurement could not be extended above 150 °C because the stiffness of the polymers fall below the minimum instrumental requirement.

In multicomponent organic polymers, measurement of glass transition temperature is a common way to detect phase separations. Fig. S2 (in Supplementary section) illustrates the temperatures of relaxation (the temperature at the maximum of tan δ, values recorded from Fig. 2) as well as the transition temperature detected by DSC measurements. It is interesting to note that the T_gs of PHA and PMMA blocks depend on the molecular weight of the outer blocks, the inner block length being unchanged ($M_n = 20$ K). As the PMMA molecular weight is increased from 10,000 to 80,000 and the PMMA content from 33 to 80%, T_gI decreases from −39 to −53 °C and T_gII increases from 131 to 140 °C. This observation is consistent with some partial miscibility of PMMA and PHA, which decreases when the length of PMMA is increased, the molecular weight of PHA being kept unchanged. This kind of partial miscibility between acrylate–methacrylate blocks has also been reported in the earlier literature [34]. As there is a probability of DMTA measurements to be dependent on frequency [35,36], hence the T_g values determined by DSC are also included in the Figure. In the present case, the T_g of PMMA determined by DSC appears about 40 °C and that of PHA about 25 °C lower than that determined by DMTA. This is in line with the earlier observations made with different polymers [37].

3.3. Tensile properties

Fig. 3 compares the stress–strain curves for a series of MHM triblock copolymers consisting of the same PHA block (20,000)

Table 2
Summary of dynamic mechanical properties of block copolymers at different temperatures.

Sample designation	log G′ (Pa)			tan δ_{max}	
	T_g I	T_g II	RT	T_g I	T_g II
(a) 5-20-5	7.8	6.21	6.95	1.32	0.81
(b)10-20-10	8.42	6.75	8.01	0.24	1.14
(c) 20-20-20	8.68	6.89	8.32	0.09	1.19
(d) 40-20-40	8.76	6.99	8.51	0.05	1.38
(e) 20-40-20	8.31	6.82	7.83	0.42	1.16

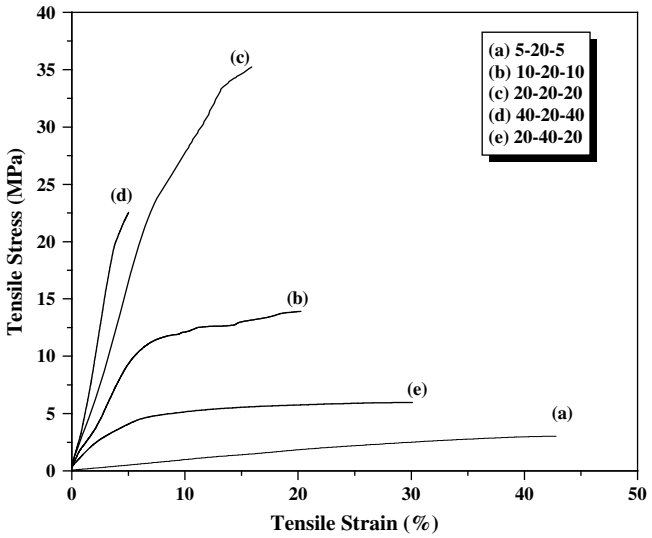

Fig. 3. Tensile stress–strain curves for MHM triblocks.

associated with PMMA blocks of increasing values of M_n (10,000–80,000) (sample a–d). The variation of chain length of the middle block has also been explored (sample e). Respective values of the tensile strength (T.S.), percent elongation at break (E.B.) and Young's modulus (tensile modulus at 2% strain) are plotted in Fig. 4. The results delineate that as the PMMA content increases; there is a gradual increase in the T.S. (except in case of sample d, PMMA content 80%) and a decrease in E.B., as it is the case for most TPEs. As expected, a constant increase in Young's modulus is observed with increasing hard phase. The dependence of T.S. on PMMA chain length up to PMMA molecular weight 40,000 suggests partial miscibility of the two polyacrylate blocks. However, when PMMA molecular weight exceeds 40,000, the T.S. of MHM gets decreased (sample d, Fig. 3) because of the very high content of hard phase. The comparison between the samples c and e indicates that although the end block length is same in both the cases, the middle block length (of PHA) is higher in sample e, which accounts for higher E.B. (30%) and lower T.S. (6 MPa), attributed to a change in phase morphology, discussed afterwards. These findings suggest a convenient way for tuning the material properties by simply adjusting the copolymer composition.

Although partial miscibility of low molecular weight PMMA and PHA blocks might partly explain the poor mechanical properties of MHM triblocks compared to that of the traditional dienes[4b], having similar hard–soft–hard compositions, the most reasonable explanation can be found in the average molecular weight between chain entanglements, M_e, of the polyacrylate central block. In this case, M_e of PHA has been determined to be 61,000 from DMTA (e.g., for sample c), which is indeed, much higher than for polydienes. M_e for the polyalkylacrylates have actually been calculated from Eqn. (1) [38]

$$M_e = \rho RT/G_N^0 \quad (1)$$

where $G^0{}_N = G'$ ($\tan\delta \rightarrow \min$) is the shear modulus in the plateau region, ρ the polymer density, R the gas constant and T the temperature. The M_e value is reasonably higher than the molecular weight of central PHA block ($M_n = 20{,}000$) in MHM copolymers, hence entanglement density is low. In this way, since the number of chain entanglements is limited in the MHM systems, the deformation stress is not dissipated by the soft PHA block but directly transferred to the hard PMMA nanodomains.

3.4. Morphology

Atomic force microscopy (AFM) appears as a unique tool for investigating the microscopic morphology of these "all-acrylate" triblock copolymers. This is because, on one hand, the electron density difference between the different monomer units is too small to measure and, on the other hand, no selective staining agent is available, which precludes morphological characterization by means of classical techniques of transmission electron microscopy and small-angle X-ray scattering [31].

The phase detection (PD) images of samples corresponding to the compositions 5-20-5, 20-20-20, 40-20-40 and 20-40-20 (Table 1) are displayed in Fig. 5a–d, respectively. Fig. 5d (of composition 20-40-20) corresponds to the sample with longer middle block length

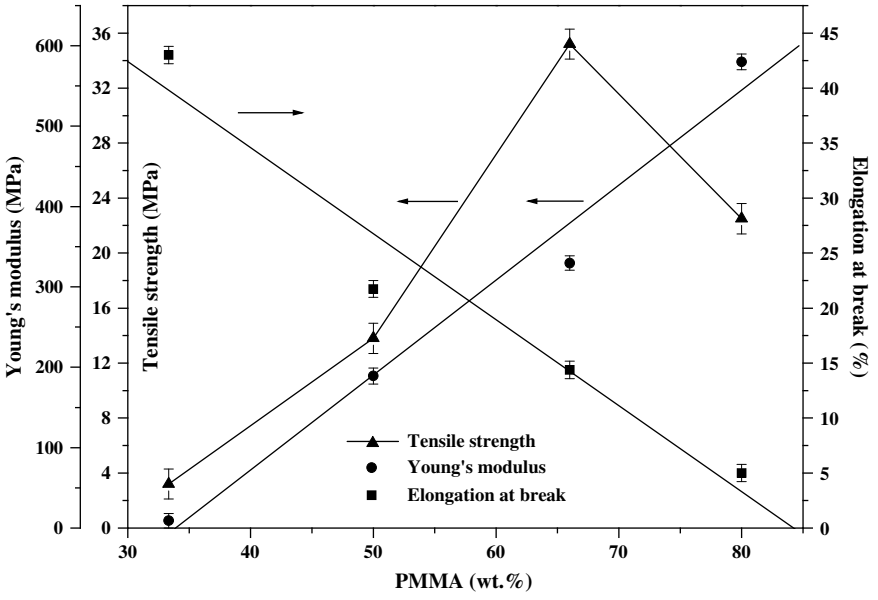

Fig. 4. Plots of tensile strength, elongation at break and Young's modulus vs. wt.% of PMMA (Error bar shows the standard deviation).

(M_n of PHA = 40 K in contrast to sample a–c, where M_n of PHA = 20 K). All these films were cast from THF. According to the previous studies of AFM images for MAM copolymers (A = alkyl acrylate) by Tong et al., the brighter areas are typical of component of higher modulus, i.e., PMMA, whereas the darker areas are the signature of the softer component [31,34]. The same assignment holds here. The elongated bright objects, identified as PMMA cylinders are either standing perpendicular or lying flat parallel to the surface, inside the continuous rubbery matrix (PHA). It should be emphasized that irrespective of compositions, all the triblock copolymers develop a well-defined nanophase separated morphology.

A representative height image on the same area of the film for the sample of composition 5-20-5 is also shown (Fig. 5e). The height image is featureless. The root-mean square (rms) roughness for a $330 \times 330\ nm^2$ area is 1.10 nm. The film surface is therefore smooth enough not to influence the PD image contrast owing to the difference in the surface topography. The surface roughness is of the same order for all the films represented here.

Fig. 5a and b displays a majority of short-range ordered cylinders and a few dots embedded in a dark continuous matrix. With increase in PMMA content (80%), sample 5c exhibits a highly textured mixed morphology. Effect of the soft block length is evidenced in Fig. 5d; the hard block domains appear to form a lamellar

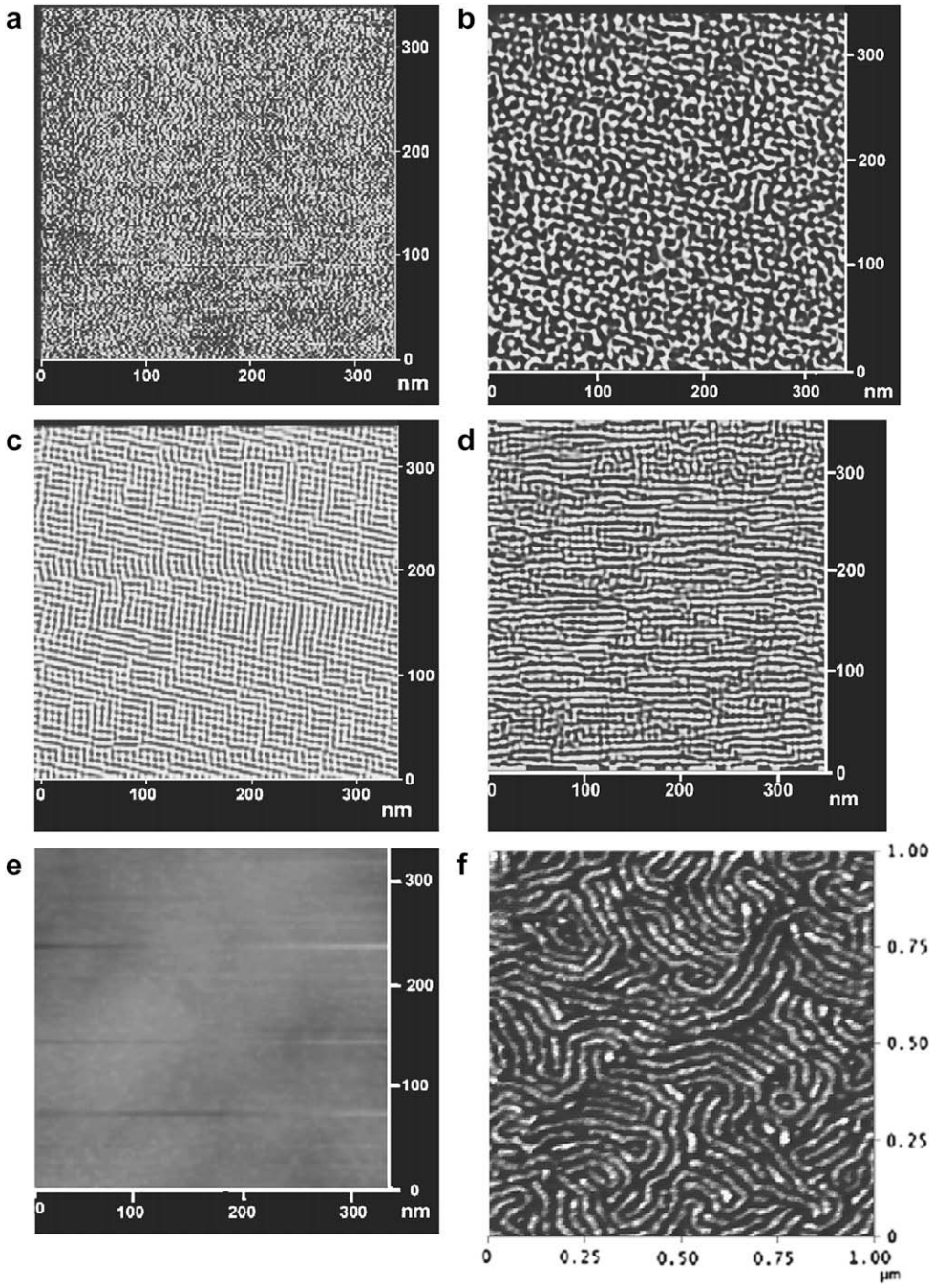

Fig. 5. Tapping mode AFM images of the MHM block copolymers. Parts a–d are phase detection images for THF cast films containing 33, 66, 80 and 50% PMMA content respectively. Part e is the height image corresponding to part a. Part f represents the annealed sample with 66% PMMA content.

ordering. The PMMA blocks are aligned in a paralleled fashion connected to each other in a percolation network in a continuous rubbery matrix. This well ordered morphology explains the extended rubbery plateau as observed in dynamic mechanical analysis (Fig. 1, sample e). Comparing samples 5c and 5d, it is evident that when the soft middle block length is higher (as in case of 5d), the sample give predominantly 'cylinders on surface' morphology, whereas when PMMA block length gets longer (as in case of 5c), 'cylinder tips on surface' morphology becomes predominant. This feature can be explained in terms of the difference in surface energy between hard and soft components. Hard block PMMA has higher surface energy (43 mJ/cm^2) compared to soft polyacrylates [39]. Henceforth, the material with higher PMMA content tends to orient in such a way that the amount of PMMA is minimized at the surface. This is possible when the PMMA cylinders stand vertically and appear as dots so that as to minimize their contact with air.

In order to have a stronger insight onto the surface morphology, before doing AFM, one representative sample was annealed at 140 °C for 24 h in vacuum (Fig. 5f).

At this temperature, which is higher than the glass transition temperature of both the blocks, a morphological transformation occurs, the immiscibility of the different blocks increases. This results in an enhanced degree of phase separation, which designates a cylinder diameter of 19.8 nm for the PMMA domain.

Similar change in surface morphology of blocks after annealing has also been reported by earlier authors [40].

3.5. Stabilization of gold nanoparticles (AuNP) by MHM triblocks

The advantages of using polymers as AuNP stabilizers are not only the enhancement of long-term stability, adjustment of the solubility and amphiphilicity of AuNPs, but also the functionalization of AuNPs with polymers to tailor their properties, as well as to promote compatibility and processibility [41].

Fig. 6 shows the UV–vis absorption characteristics of the as prepared gold–MHM nanocomposite thin films. The sample with 33% PMMA content (spectrum a) is proven to be a poor mediator for stabilizing gold NP's as indicated by the absence of any absorption peak in the visible region. With increasing PMMA content, an absorption band with $\lambda_{max} = 538$ nm develops, known to originate from the Surface Plasmon Resonance absorption, the position and shape of which is a function of the aspect ration of the nanocrystals formed. In case of composite with PMMA content 50% and 66.6% (spectra b,c), one can see a symmetrical SPR absorption bands which refers to stabilization

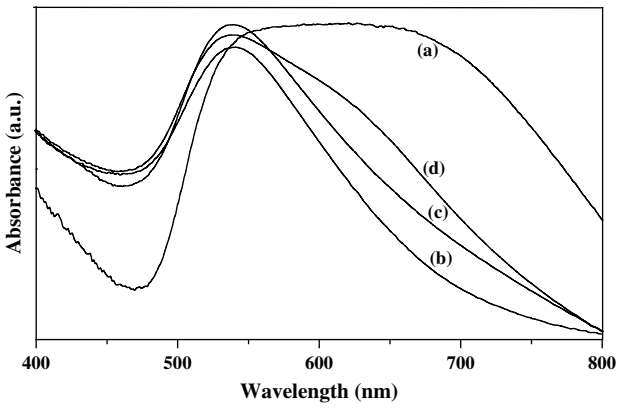

Fig. 6. UV–vis absorption spectra of Au nanoparticles prepared in DMF using MHM block copolymers as stabilizer; (a) 5-20-5, (b) 10-20-10, (c) 20-20-20, (d) 40-20-40.

of spherical gold nanoparticles. As the PMMA content is increased further to 80%, a shoulder at 650 nm appears along with the 538 nm peak, indicating the possible presence of some oblate shaped gold nanoparticles (see in TEM section). This phenomenon is well known for high aspect ratio nanocrystals. As the aspect ratio increases from 1, the resonance frequency splits into two distinct energy levels. The high energy band corresponds to the oscillation of electrons perpendicular to the major axis and is referred to as transverse plasmon absorption. The other absorption band which is red shifted to low energy arises due to oscillation of electrons along the major axis [42]. Shipaway et al. [41c] reported that gold nanoparticle aggregation might also result in longitudinal plasmon resonance due to interparticle plasmon coupling.

TEM images provide direct visualization of the structures of the as prepared AuNPs. Fig. 7 show the TEM images and size distributions of samples. As displayed in Fig. 9a, when the stabilizer polymer block contains PMMA content 66%, there develops closely packed nanoparticle aggregates of an ensemble of particles. The stabilized nanoparticles are mostly spherical and uniform in size, as proposed by the symmetrical nature of their corresponding UV–vis spectra. It also appears from an enlarged view of a portion of the assembly (inset of Fig. 7a) that most of the adjacent nanoparticles are in close contact and interparticle distances are less than the average particle diameter.

When the stabilizer was switched to the triblock, which has PMMA content of 80%, a three dimensional network of nanoparticle aggregates is generated (Fig. 7b). This particular assembly contains NPs of varying size distribution with a deviation in spherical shape; some particles get elongated to certain directions (inset of Fig. 7b), supporting also their respective surface plasmon. Fig. 7c shows the histogram of the gold NPs in Fig. 7a. A narrow size distribution of the nanoparticles is clear and the statistical analysis shows that the maximum number of particles have the average size around 11.6 ± 1.2 nm.

Earlier study [43] shows that PMMA has a very good interaction with metal nanoparticles. Hence, it may be rationalized that when the polymer contains a reasonably higher content of PMMA (80%), growth of NPs is inhibited at the polymeric anchor points so that the particle growth becomes nonuniform. It has been reported by Tannenbaum et al. [43] that iron oxide nanoparticles synthesized in the weakly interacting PS are spherical, while those formed in strongly interacting PMMA are pyramidal. Following the similar argument it can be stated that it is the higher PMMA content of the MHM stabilizer (in this case 80%) that lead to the NPs deviated from spherocity (as displayed in Fig. 7b).

The sample of the gold nanoaggregates was further confirmed by Energy-dispersive X-ray spectroscopy (EDS) analysis as shown in Fig. S3 (Supplementary section). No other element is detected by EDS, indicating that these aggregated structures are purely gold. The inset Figure shows the selected-area electron diffraction (SAED) pattern of polymer-stabilized AuNPs, which clearly demonstrates that gold aggregates are polycrystalline in nature.

To establish whether the aggregates are actually forming in the solution and not during the drying process of the sample on the TEM grid, dynamic light scattering (DLS) measurement was performed with the polymer–AuNP suspension in DMF. DLS data (Fig. S4 in Supplementary section) explains that the hydrodynamic diameter (79 nm) of the aggregated AuNPs is much greater than that of the isolated nanoparticles (11.6 nm). This indicates that the aggregation occurs in the reaction medium and not during solvent drying on the TEM grid.

To analyze the possible physicochemical interaction between AuNP and polymer matrix, FTIR was carried out. Fig. 8 displays a selected part of the absorbance infrared spectra of neat polymer

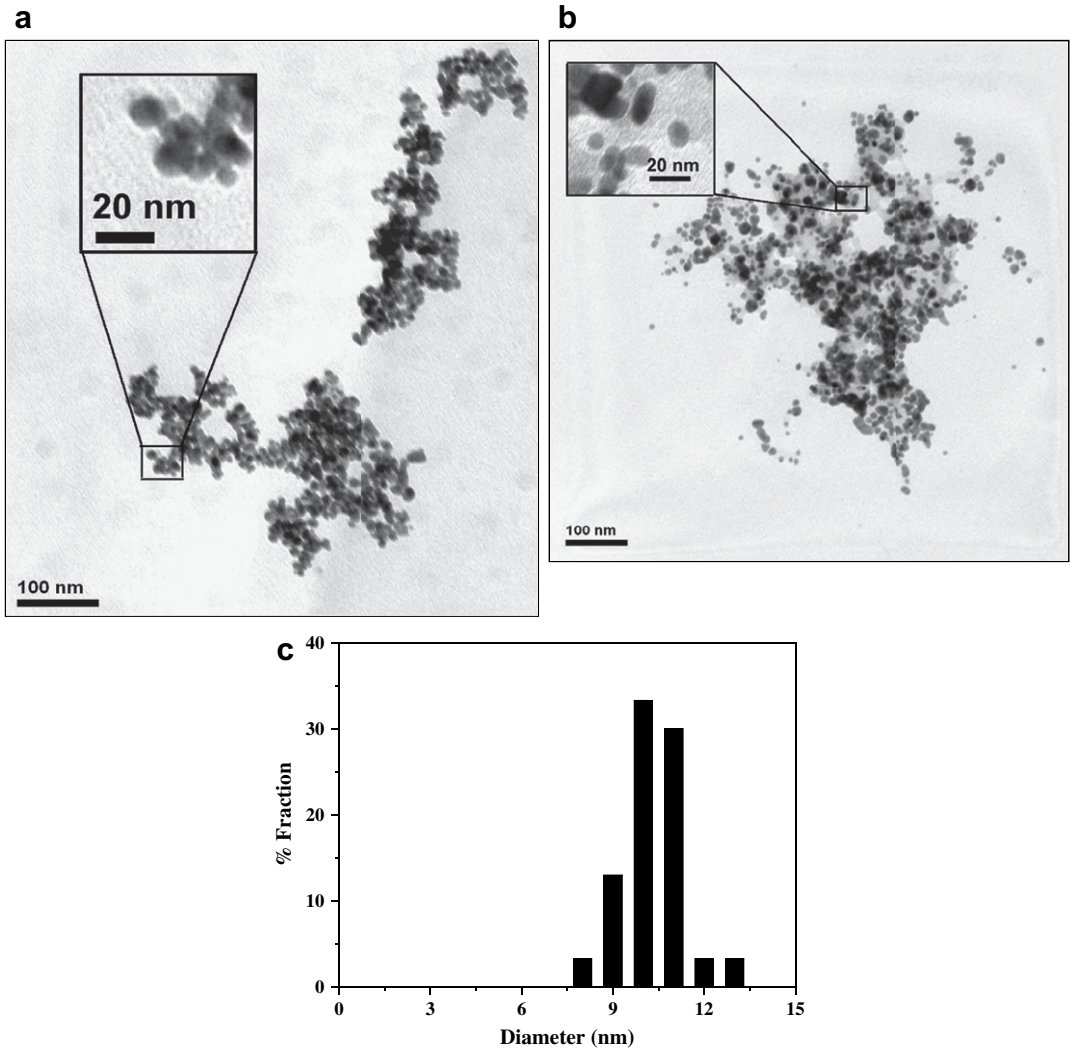

Fig. 7. TEM micrographs of polymer-stabilized AuNPs stabilized by different polymers (a) PMMA content: 66%, (b) PMMA content: 80%. (c) Size histogram of the gold NPs synthesized in part a.

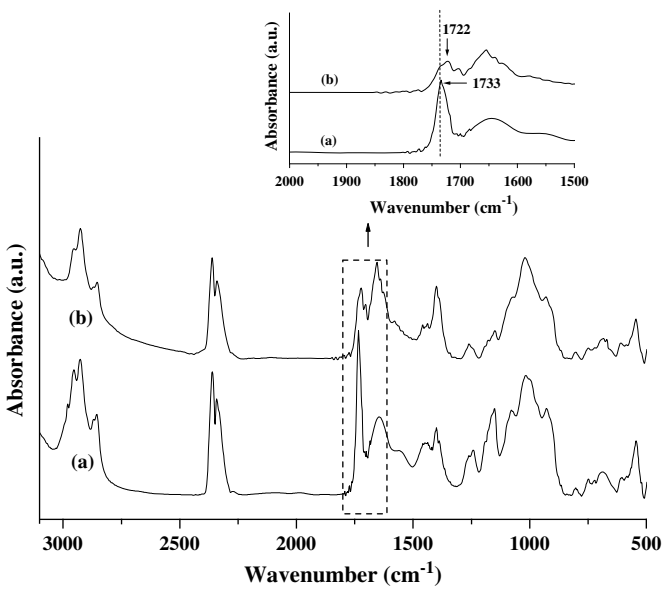

Fig. 8. FTIR image of (a) Neat polymer and (b) Polymer–Au nanocomposite.

a (MHM, 20-20-20) and polymer capped Au nanoparticles b, both are taken in DMF. The neat MHM spectrum shows a strong absorbance at 1733 cm^{-1} that is characteristic of the >C═O stretching, and absorbance at 1400–1500 cm^{-1} and 2800–3000 cm^{-1} regions that are characteristics of the C–H bending and stretching, respectively [44]. The peak at 1652 cm^{-1} might be attributed to the presence of free DMF. The frequency of carbonyl group (>C═O) stretching in polymer capped Au nanoparticles is shifted to 1722 from 1733 cm^{-1} of that in neat polymer, along with a considerable decrease and broadening in peak height. It has been calculated that in b, there is a reduction in peak area (under >C═O str.) by 35% (normalization against the peak at 2927 cm^{-1}, C–H stretching). These results indicate that the MHM molecules adsorb on the surface of the gold nanoparticles, probably due to the coordination between gold and oxygen atom of the carbonyl groups in MHM. Similar type of interaction of PMMA with other metal nanoparticle through the >C═O functional group has already been established [46].

An important and major aspect of these block copolymer stabilized nanoparticles is the preparation of polymer–metal nanocomposites (PNCs). MHM stabilized Au nanoparticles could be successfully used for the preparation of Au–polymer nanocomposite films with hydrophobic polymers. For the present study,

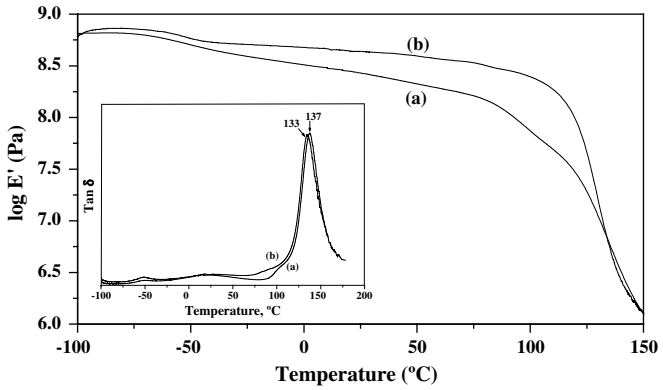

Fig. 9. Dynamic Mechanical analysis of (a) neat polymer and (b) its Au-filled nanocomposite.

the block copolymer stabilized gold nanoparticles were successfully blended with MHM block copolymer matrix of composition 20-20-20 (sample c, Table 1). The as prepared film was transparent and had the same color as that of respective Au nanoparticles prepared in solution (see the photograph in supporting information, Fig. S5).

The incorporation of fillers into a polymer matrix can bring about changes in the mechanical and thermal characteristics of the resulting composite. One benchmark that is used to compare the dynamical mechanical behavior of PNCs is the storage modulus. The mechanical reinforcement of nanofiller in the polymer matrix can be visualized well from the storage modulus in Fig. 9, where the storage modulus of neat and filled polymer is plotted as a function of temperature. It has been calculated that there is about 1.9% increase of E' for PNC at 0 °C, 2.5% at 25 °C and 6.7% at 100 °C. The degree of enhancement in E' is more distinct near the glass transition of hard phase, whereas near the soft range it is quite trivial. It implies that the nanoparticles have reinforced the hard block more effectively in accordance with the prior literature report on interaction of gold nanoparticles with PMMA [44,45]. This is quite obvious as the >C=O group of PMMA is easily accessible for interaction with metal compared to that of PHA due to lesser steric hindrance in the former case.

In order to further elucidate the role of PMMA in stabilizing AuNPs, we prepared a model triblock copolymer taking polystyrene (PSt) as the hard and PHA as the soft segment, i.e., PSt-b-PHA-b-PSt (of composition 20-20-20). This material failed to perform as a stabilizer for preparing gold particles in nanodimension. Henceforth, the role of PMMA is established.

The tensile strength of the nanocomposite also increased from 34.5 MPa in neat polymer to 35.2 MPa, as expected with a marginal sacrifice in E.B. (from 16% in neat polymer to 14% in PNC). The inset of Fig. 9, (i.e., the tan δ vs. temperature plot) indicates that there is a decrease in the glass transition temperature by 4 °C for the hard segment. Most researchers in this field have reported almost no variation in the T_g as a function of filler content; however, a decrease in the T_g has also been reported in the case of alumina/PMMA nanocomposite [46].

Fig. S6 (in Supplementary section) displays the typical TGA thermograms of weight loss as a function of temperature of neat MHM copolymer (PMMA content 66%) and its Au-filled nanocomposite measured under nitrogen atmosphere. The onset of degradation, as calculated from the intersection of the tangent of the initial part and the inflection part increases from 304 °C in neat polymer to 316 °C in PNC indicating an enhancement in thermal stability in presence of AuNPs.

3.6. Conclusion

A series of PMMA-b-PHA-b-PMMA (MHM) triblock copolymers of various molecular weights and compositions have been prepared by ATRP using soft PHA ($T_g = -57$ °C) as the middle block and hard PMMA ($T_g = 100$ °C) as the outer blocks. Solution cast films of MHM triblocks are characterized by SEC, DSC, DMTA, AFM analysis and tensile properties. DMTA analysis reveals two glass transitions and an intermediate rubbery plateau for all block copolymers, which is in agreement with extended phase separation. The mechanical and tensile properties of MHM triblocks are somewhat affected due to the partial miscibility of blocks as well as high value of M_e for PHA. It is evident from the morphological study that when the soft middle block length is higher, the samples give primarily 'cylinders on surface' morphology, whereas when PMMA block length gets longer, 'cylinder tips on surface' morphology becomes predominant. Tensile properties of the as prepared MHM block copolymers indicate that as the PMMA content increases, the tensile strength increases and elongation at break decreases indicating their applicability as potential TPEs. Eventually, the MHM triblocks also can act as promising precursors for synthesizing organically dispersible gold nanoaggregates of core diameter about 10–15 nm which are characterized by UV–vis, TEM, FTIR DMTA and DLS analysis.

Acknowledgement

We acknowledge IIT Kharagpur for providing Fellowship and DST, New Delhi for financial support. We also thank Prof. S. Dasgupta, Department of Chem. Engg., IIT Kharagpur for carrying out DLS measurement and Prof. T. Pal, Department of Chemistry, IIT Kharagpur for helpful discussions.

Appendix. Supplementary material

Supplementary data associated with this article can be found in the online version at doi:10.1016/j.polymer.2009.04.071.

References

[1] (a) Estes GM, Cooper SL, Tobolsky AV. J Macromol Sci 1970;C4:313;
(b) Holden G, Legge NR. In: Holden G, Legge NR, Quirk R, Schroeder HE, editors. Thermoplastic elastomers. 2nd ed. Munich, Germany: Hanser; 1996;
(c) Morton M. In: Legge NR, Holden G, Schroeder HE, editors. Thermoplastics elastomers – a comprehensive review. Munich, Germany, Vienna, and New York: Hanser; 1987 [chapter 4];
(d) Krasia T, Soula R, Börner HG, Schlaad H. Chem Commun 2003:538.
[2] (a) Hadjichristidis N, Pispas S, Floudas G. In: Block copolymers: synthetic strategies, physical properties, and applications. Chichester, UK: J. Wiley & Sons; 2002;
(b) Bhowmick AK, Stephens HL. Handbook of elastomers. New York: Marcel Dekker; 2001;
(c) Jerome R, Fayt R, Teyssie P. In: Legge NR, Holden G, Schroeder HE, editors. Thermoplastic elastomers. Munich, Germany: Hanser; 1987;
(d) Dufour B, Tang C, Koynov K, Zhang Y, Pakula T, Matyjaszeski K. Macromolecules 2008;41:2451.
[3] (a) Gallot BRM. Adv Polym Sci 1978;29:85;
(b) Hashimoto T, Nagatoshi K, Todo A, Hasegawa H, Kawai H. Macromolecules 1974;7:364.
[4] (a) Tong JD, Leclere Ph, Doneux C, Bredas JL, Lazzaroni R, Jerome R. Polymer 2000;41:4617;
(b) Tong JD, Jerome R. Polymer 2000;41:2499;
(c) Moineau C, Minet M, Teyssie P, Jerome R. Macromolecules 1999;32:8277;
(d) Kitayama T, Ogawa M, Kawauchi T. Polymer 2003;44:5201.
[5] (a) Shipp DA, Wang JL, Matyjaszewski K. Macromolecules 1998;32:4482;
(b) Jeusette M, Leclere Ph, Lazzaroni R, Simal F, Vaneecke J, Lardot Th, et al. Macromolecules 2007;40:1055;
(c) Matyjaszewski K, Shipp DA, Mcmurtry Gaynor SG, Pakula T. J Polym Sci Part A Polym Chem 2000;38:2023;
(d) Cowie JMG, Ferguson R, Fernandez MD, Fernandez MJ, McEwen IJ. Macromolecules 1992;25:3170;
(e) Matyjaszewski K. Macromolecules 2003;36:8969.
[6] (a) Matyjaszewski K, Xia J. Chem Rev 2001;101:2921;
(b) Kamigaito M, Ando T, Sawamoto M. Chem Rev 2001;101:3689;
(c) Yin M, Habicher WD, Voit B. Polymer 2005;46:3215;

(d) Sadhu VB, Pointeck J, Voit B. Macromol Chem Phys 2004;205:2;
(e) Adam L, Haddleton DM. Macromolecules 2006;39:1353;
(f) Street G, Illsley D, Holder SJ. J Polym Sci Part A Polym Chem 2005;43:1129;
(g) Harries HV, Holder SJ. Polymer 2006;47:5701.
[7] (a) Percec V, Barboiu B, Kim HJ. J Am Chem Soc 1998;120:305;
(b) Moineau G, Minet M, Dubois Ph, Teyssie Ph, Senninger T, Jerome R. Macromolecules 1999;32:27.
[8] (a) Datta H, Singha NK, Bhowmick AK. Macromolecules 2008;41:50;
(b) Kavitha A, Singha NK. J Polym Sci Part A Polym Chem 2007;45:4441;
(c) Datta H, Bhowmick AK, Singha NK. J Polym Sci Part A Polym Chem 2008;46:3499;
(d) Singha NK, De Ruiter B, Schubert US. Macromolecules 2005;38:3596.
[9] Watson KJ, Zhu J, Nguyen ST, Mirkin CA. J Am Chem Soc 1999;121:462.
[10] Lai JI, Shafi KVPM, Ulman A, Loos K, Lee Y, Vogt T, et al. J Phys Chem B 2005;109:15.
[11] Skaff H, Emrick T. Angew Chem Int Ed 2004;43:5383.
[12] Sakai T, Alexandridis P. Langmuir 2004;20:8426.
[13] Savin DA, Pyun J, Patterson GD, Kowalewski T, Matyjaszewsk K. J Polym Sci Part B Polym Phys 2002;40:2667.
[14] Lowe AB, Sumerlin BS, Donovan MS, McCormick CL. J Am Chem Soc 2002;124:11562.
[15] Pyun J, Matyjaszewski K, Kowalewski T, Savin D, Patterson G, Kickelbick G, et al. J Am Chem Soc 2001;123:9445.
[16] Meli L, Li Y, Lim Kwon Teak, Johnston Keith P, Green Peter F. Macromolecules 2007;40:6713.
[17] Glomm WRJ. Dispersion Sci Technol 2005;26:389.
[18] Suzuki M, Niidome Y, Kuwahara Y, Terasaki N, Inoue K, Yamada S. J Phys Chem B 2004;108:11660.
[19] Budroni G, Corma A. Angew Chem Int Ed 2006;45:3328.
[20] Eustis S, El-Sayed MA. Chem Soc Rev 2006;35:209.
[21] Grabar KC, Smith PC, Musick MD, Davis JA, Walter DG, Jackson MA, et al. J Am Chem Soc 1996;118:1148.
[22] (a) Kneipp K, Kneipp H, Kneipp J. Acc Chem Res 2006;39:443;
(b) Pal T, Ghosh SK. Chem Rev 2007;107:4797.
[23] (a) Nam JM, Park SJ, Mirkin CA. J Am Chem Soc 2002;124:3820;
(b) Hainfeld JM, Powell RD. J Histochem Cytochem 2000;48:471;
(c) Hirsch LR, Stassord RJ, Bankson JA, Sershen SR, Rivera B, Price RE, et al. Proc Natl Acad Sci U S A 2003;100:13549.
[24] Shu Chen, Chen Guo, Guo-Hua Hu, Hui-Zhou Liu, Xiang-Feng Liang, Jing Wang, et al. Colloid and Polym Sci 2007;285:1543.
[25] Filali M, Colard C, Guillet P, Fustin CA, Soumillion P, Meier MAR, et al. Polym Prepr 2006;47:961.
[26] Filali M, Meier MAR, Schubert US, Gohy JF. Langmuir 2005;21:7995.
[27] Youk JH, Park MK, Locklin J, Advincula R, Yang J, Mays J. Langmuir 2002;18:2455.
[28] Jewrajka SK, Chatterjee U. J Polym Sci Part A Polym Chem 2006;44:1841.
[29] Karanam S, Goossens H, Klumperman B, Lemstra P. Macromolecules 2003;36:3051.
[30] Moineau G, Minet M, Teyssie Ph, Jerome R. Macromol Chem Phys 2000;201:1108.
[31] Tong JD, Leclere Ph, Rasmont A, Bredas JL, Lazzaroni R, Jerome R. Macromol Chem Phys 2000;201:1250.
[32] Chatterjee DP, Mandal BM. Macromolecules 2006;39:9192.
[33] Brandrup J, Immergut EH. Polymer handbook. 2nd ed. New York: Wiley-Interscience; 1975.
[34] Tong JD, Leclere Ph, Doneux C, Bredas JL, Lazzaroni R, Jerome R. Polymer 2001;42:3503.
[35] Nielson LE. Mechanical properties of polymers and composites. New York: Marcel Dekker; 1974.
[36] Ma X, Sauer JA, Hara M. Macromolecules 1995;28:3953.
[37] Bhowmick AK. In: Rawlings ED, editor. Materials science and engineering, encyclopedia of physical sciences, engineering and technology, Chapter 1, Eloss Publishers, Oxford, UK; 2002.
[38] Ferry JD. Viscoelastic properties of polymers, vol. 3. New York: Wiley; 1980.
[39] Van Krevelen DW. Properties of polymers, vol. 3. Amsterdam: Elsevier; 1990. p. 790.
[40] (a) Liang GD, Xu J-T, Fan Z-Q. J Phys Chem B 2007;41:11921;
(b) Fang H, Feng L, You B, Wu L. J Polym Sci Part B Polym Phys 2007; 45:208.
[41] (a) Shan J, Tenhu H. Chem Commun 2007:4580;
(b) Rozenberg BA, Tenne R. Prog Polym Sci 2008;33:40;
(c) Shipway AN, Lahav M, Gabai R, Willner I. Langmuir 2000;16:8789.
[42] Burda C, Chen X, Narayanan R, El-Sayed MA. Chem Rev 2005;105:1025.
[43] Tannenbaum R, Zubris M, Goldberg EP, Reich S, Dan N. Macromolecules 2005;38:4254.
[44] Nyquist RC. Interpreting infrared, Raman, and nuclear magnetic resonance spectra, vol. 1. New York: Academic Press; 2001.
[45] Guo Z, Henry LL, Palshin V, Podlaha EJ. J Mater Chem 2006;16:1772.
[46] Ash BJ, Siegel RW, Schadler LS. Macromolecules 2004;37:1358.